

*Supporting Information*

**Residue-Specific Solvation Directed Thermodynamic and Kinetic Control over Peptide Self-assembly with 1D/2D Structure Selection**

Yiyang Lin,<sup>†</sup> Matthew Penna,<sup>‡</sup> Michael R. Thomas,<sup>†</sup> Jonathan P. Wojciechowski,<sup>†</sup> Vincent Leonardo,<sup>†</sup> Ye Wang,<sup>†</sup> E. Thomas Pashuck,<sup>†</sup> Irene Yarovsky,<sup>\*,‡</sup> Molly M. Stevens<sup>\*,‡</sup>

<sup>†</sup> Department of Materials, Department of Bioengineering and Institute for Biomedical Engineering, Imperial College London, Exhibition Road, London SW7 2AZ, UK.

E-mail: [m.stevens@imperial.ac.uk](mailto:m.stevens@imperial.ac.uk)

<sup>‡</sup> School of Engineering, RMIT University, Melbourne, Victoria 3001, Australia

E-mail: [irene.yarovsky@rmit.edu.au](mailto:irene.yarovsky@rmit.edu.au)

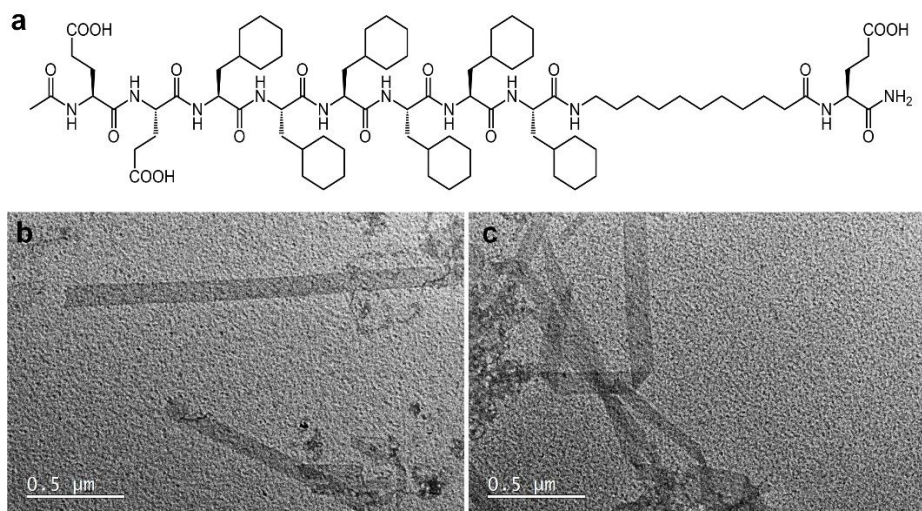


**Figure S1.** (a) Molecular structure of a mutated peptide where phenylalanine is replaced by 3-cyclohexyl-*L*-alanine. (b, c) Representative TEM images of self-assembled nanobelts formed by mutated peptide (0.25 mM) in phosphate buffer (10 mM, pH 7.0).

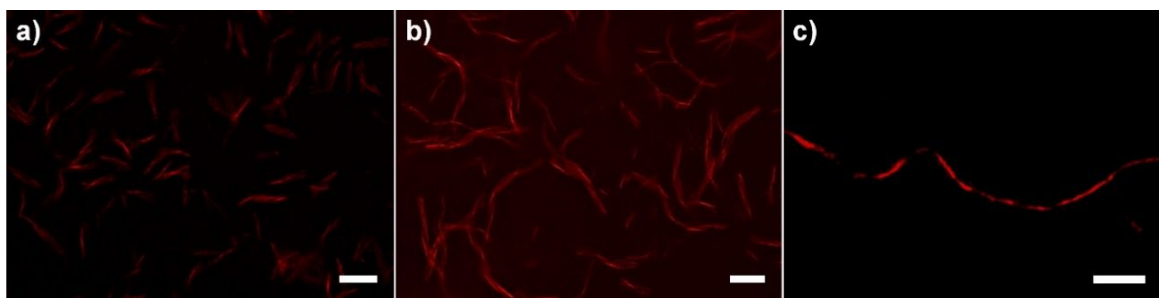


**Figure S2.** Structured illumination microscopy images of F6C11 (0.25 mM) self-assembly, showing the transition from 2D nanosheets to elongated nanobelts and 1D nanofibrils. The volume concentration of methanol was (a) 5 v/v%; (b) 10 v/v%; (c) 15 v/v%. The peptide nanostructures were stained with hydrophobic Nile Red (2.5  $\mu$ M). Scale bar: 2  $\mu$ m.

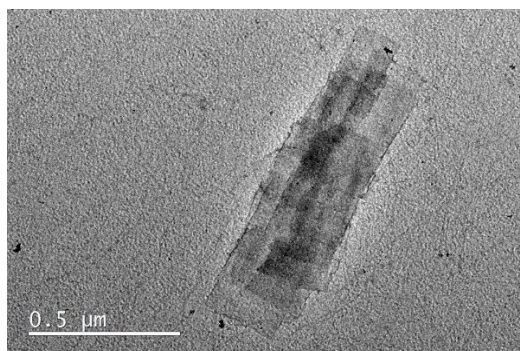


**Figure S3.** TEM image of F6C11 nanosheets formed from cosolvent exchange. The fibrils were initially formed with 15% of methanol aqueous solution, and dialyzed against phosphate buffer (10 mM, pH 7.0) to remove methanol.

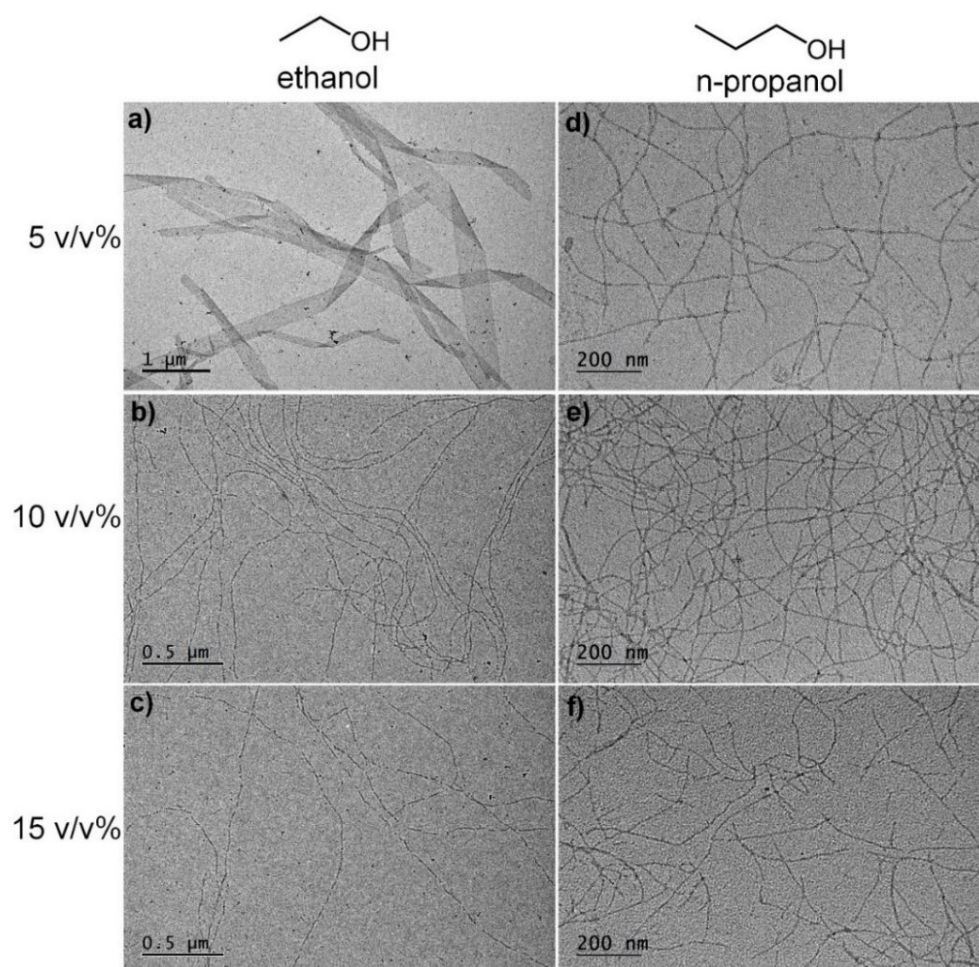


**Figure S4.** TEM images of F6C11 (0.25 mM) self-assembly in the presence of (a-c) ethanol and (d-f) *n*-propanol in phosphate buffer (10 mM, pH 7.0). The volume concentration of cosolvents was (a, d) 5 v/v%; (b, e) 10 v/v%; (c, f) 15 v/v%. The presence of 5 v/v% ethanol favors the formation of elongated peptide nanobelts, similar to that observed for 10 v/v% methanol. In contrast, the presence of 5 v/v% *n*-propanol induces the formation of amyloid-like fibrils.

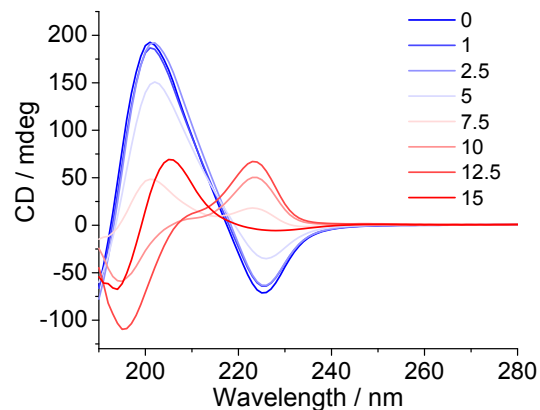


**Figure S5.** CD spectra of F6C11 solution in the presence of ethanol. The volume concentration of cosolvent was 0, 1 %, 2.5 %, 5 %, 7.5 %, 10 %, 12.5 % and 15 %.

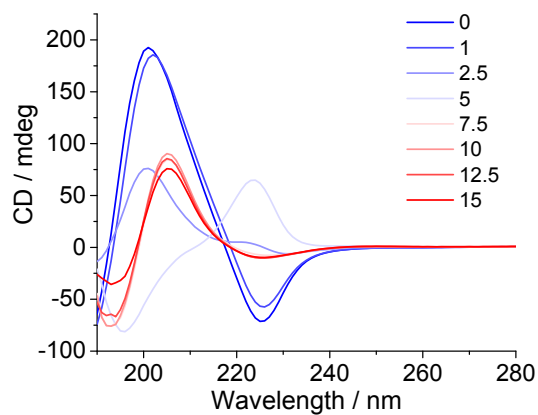


**Figure S6.** CD spectra of F6C11 solution in the presence of *n*-propanol. The volume concentration of cosolvent was 0, 1 %, 2.5 %, 5 %, 7.5 %, 10 %, 12.5 % and 15 %.

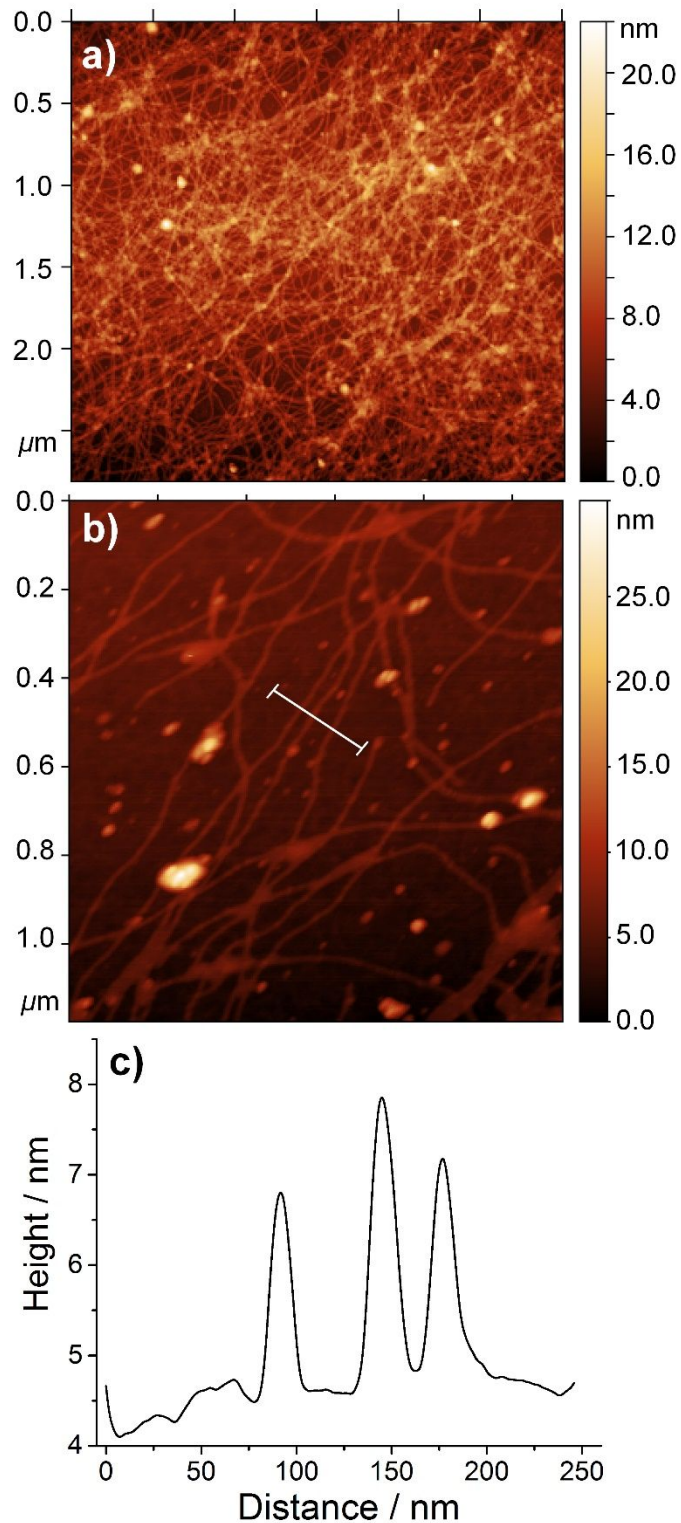


**Figure S7.** (a) A representative atomic force microscopy (AFM) tapping-mode image showing the formation of high yield peptide fibrils in the presence of 5 % isopropanol; (b) An enlarged AFM image and (c) the height profile across the marked section indicated in (b), showing the thickness of peptide fibrils is 2~3 nm.

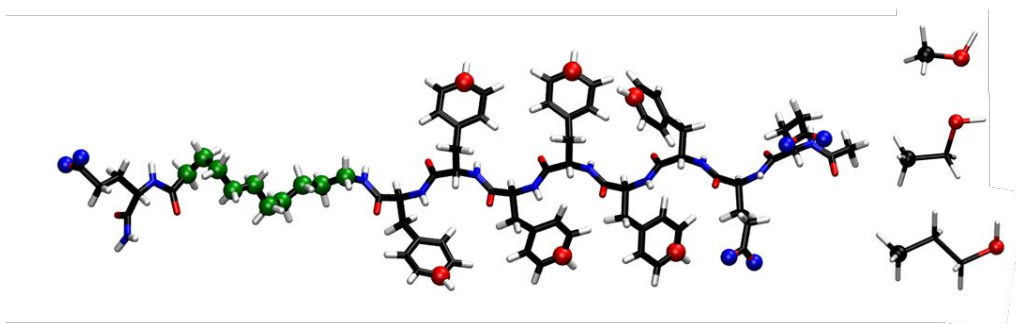


**Figure S8.** Peptide F6C11 and alcohol molecules (methanol, ethanol and *n*-propanol). Atoms shown as spheres were used in radial distribution function (RDF) calculations. For all alcohols, the oxygen and the terminal carbon were used. Due to the symmetry of the other solvents multiple solvent atoms were used in the RDF calculation. The coloured spheres in F6C11 are the reference atoms for the RDF curves in **Figures S9** and **S10**.

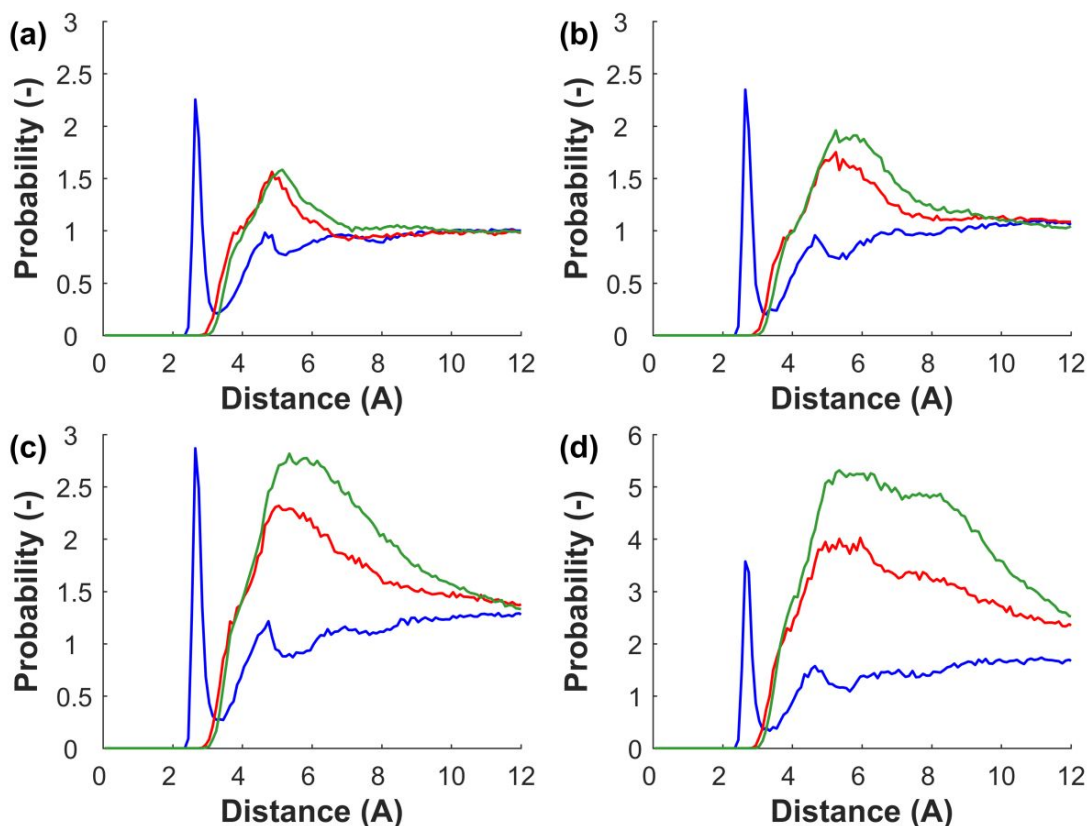


**Figure S9.** RDF between oxygen in (a) methanol, (b) ethanol, (c) *n*-propanol and (d) *n*-butanol and alkyl carbon atoms (green), aromatic carbon of phenylalanine (red) and terminal oxygen atoms of glutamic acid (blue). Reference atoms are shown as spheres in **Figure S8**. RDFs are not independent due to the small size and flexibility of the molecule.

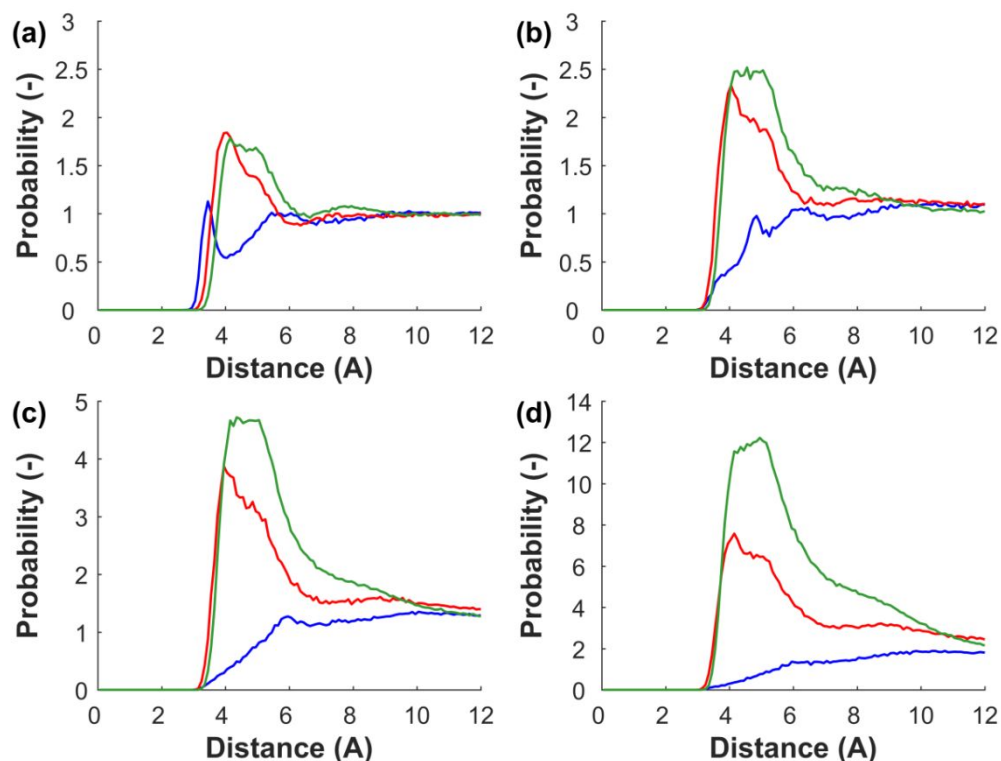


**Figure S10.** RDF between terminal carbon in (a) methanol, (b) ethanol, (c) *n*-propanol and (d) *n*-butanol and alkyl carbon atoms (green), aromatic carbon of phenylalanine (red) and terminal oxygen atoms of glutamic acid (blue). Reference atoms are shown as spheres in **Figure S8**. RDFs are not independent due to the small size and flexibility of the molecule. The association of the more nonpolar solvents (*e.g.*, *n*-propanol and *n*-butanol) with the alkyl group and Phe<sub>6</sub> peptide relative to bulk concentration is higher than polar cosolvents (*e.g.*, methanol and ethanol).

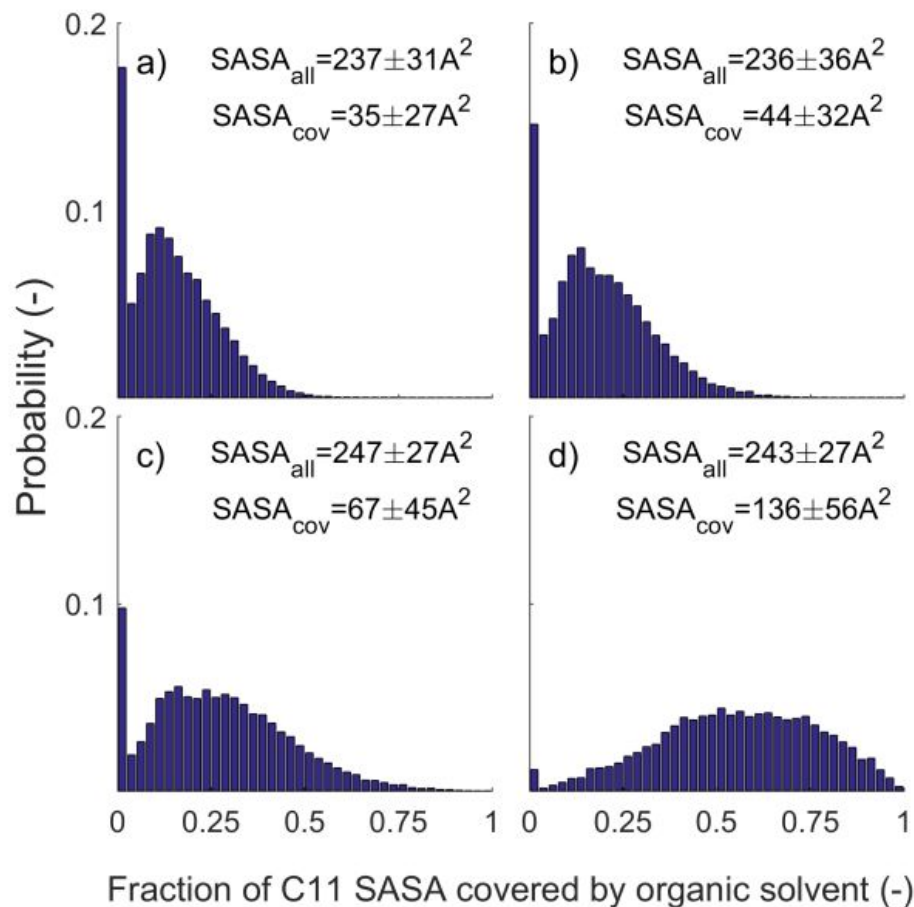


**Figure S11.** Distributions of the fraction solvent accessible surface area (SASA) of the *alkyl chain* in the F6C11 molecule covered by (a) methanol, (b) ethanol, (c) *n*-propanol, and (d) *n*-butanol with fitted normal distributions. The fraction SASA of the C11 alkyl chain covered by cosolvents increases from methanol and ethanol, to *n*-propanol and *n*-butanol.

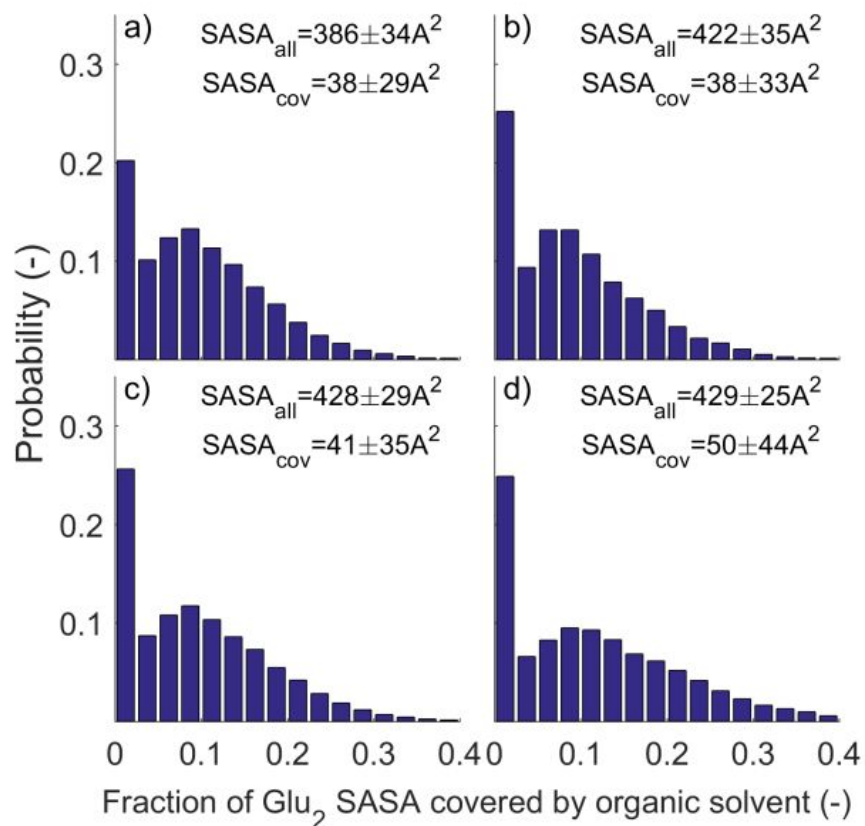


**Figure S12.** Distributions of the fraction solvent accessible surface area (SASA) of the N-terminal *Glu*<sub>2</sub> in the F6C11 molecule covered by (a) methanol, (b) ethanol, (c) *n*-propanol, and (d) *n*-butanol with fitted normal distributions. The fraction SASA of the N-terminal *Glu*<sub>2</sub> covered by cosolvents is not significantly affected by solvent polarity.

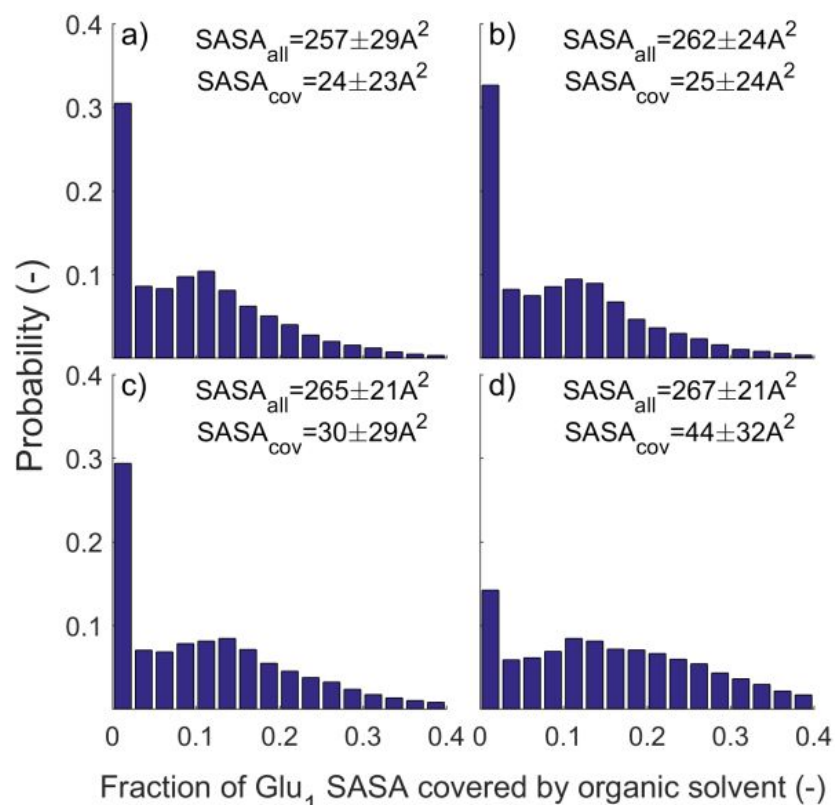


**Figure S13.** Distributions of the fraction solvent accessible surface area (SASA) of the C-terminal *Glu* in the F6C11 molecule covered by (a) methanol, (b) ethanol, (c) *n*-propanol, and (d) *n*-butanol with fitted normal distributions. The fraction SASA of the C-terminal *Glu* covered by cosolvents is not significantly affected by solvent polarity.

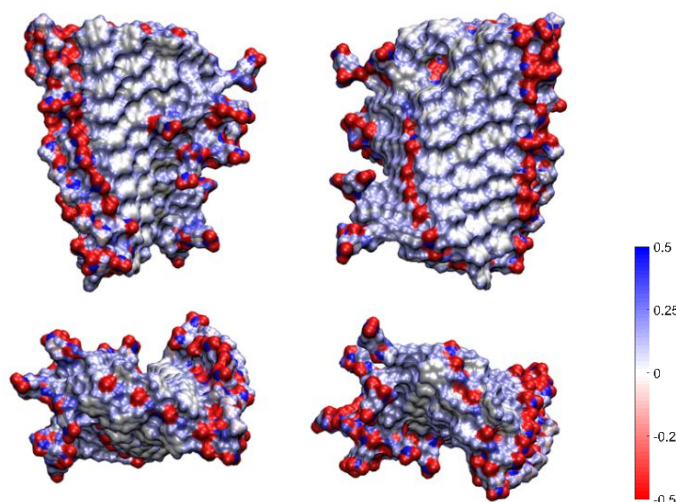


**Figure S14.** F6C11<sub>10</sub> protofibril shown as a surface with atoms coloured according to charge with a colour range of -0.5 (red), 0.0 (white) and +0.5 (blue). The two walls of the protofibril (top) and the two ends (bottom) are shown. The hydrophobic wall is the white region seen in the top two figures and the red dots along the ends of the bottom are the peptide backbone.

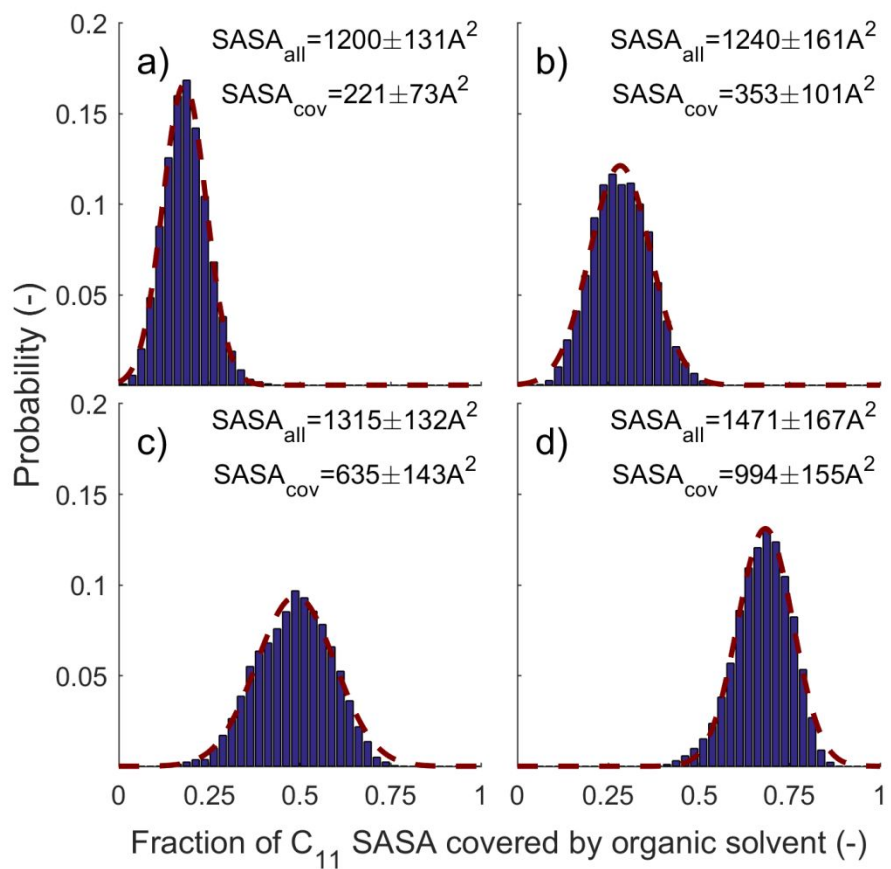


**Figure S15.** Distributions of the fraction solvent accessible surface area (SASA) of the *alkyl chain* in the F6C11<sub>10</sub> protofibril covered by (a) methanol, (b) ethanol, (c) *n*-propanol, and (d) *n*-butanol with fitted normal distributions. The fraction SASA of the C<sub>11</sub> alkyl chain covered by cosolvents increases from methanol and ethanol, to *n*-propanol and *n*-butanol.

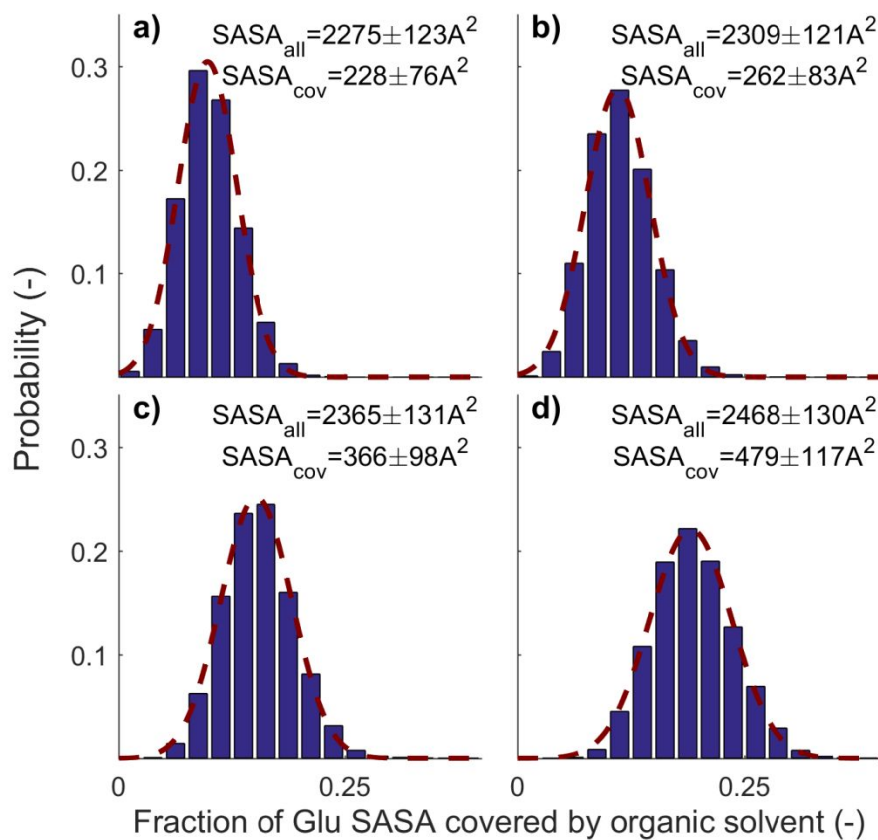


**Figure S16.** Distributions of the fraction solvent accessible surface area (SASA) of the C-terminal *Glu* in the F6C11<sub>10</sub> protofibril covered by (a) methanol, (b) ethanol, (c) *n*-propanol, and (d) *n*-butanol with fitted normal distributions. The fraction SASA of the C-terminal *Glu* covered by cosolvents is not significantly affected by solvent polarity.

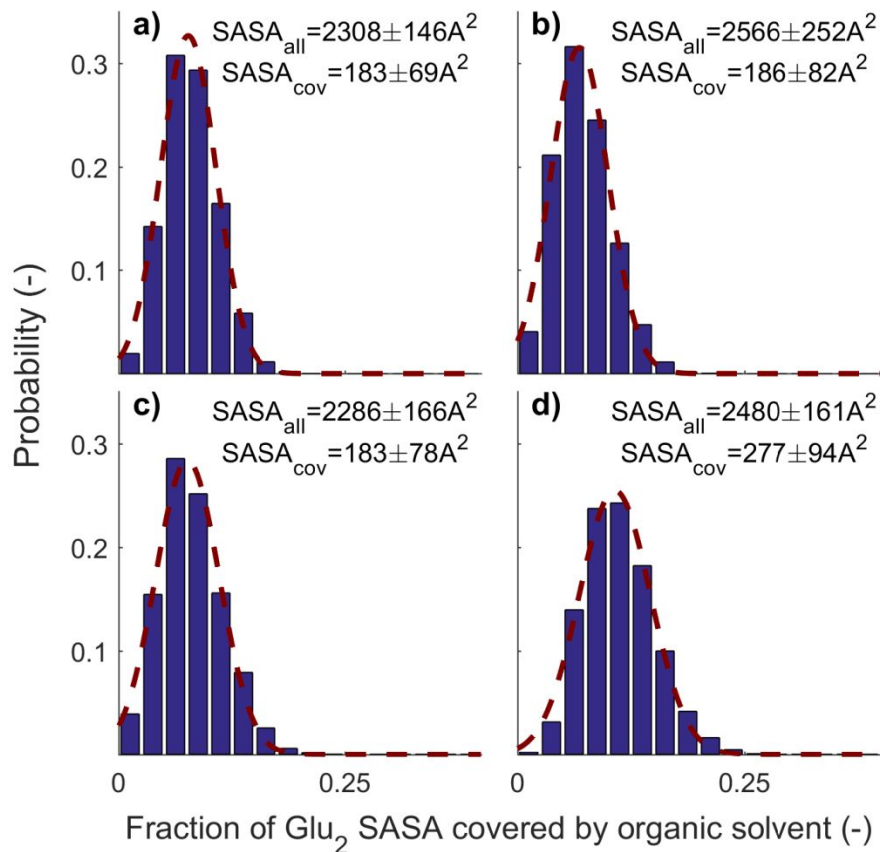


**Figure S17.** Distributions of the fraction solvent accessible surface area (SASA) of the N-terminal  $Glu_2$  in the F6C11<sub>10</sub> protofibril covered by (a) methanol, (b) ethanol, (c) *n*-propanol, and (d) *n*-butanol with fitted normal distributions. The fraction SASA of the N-terminal  $Glu_2$  covered by cosolvents is not significantly affected by solvent polarity.

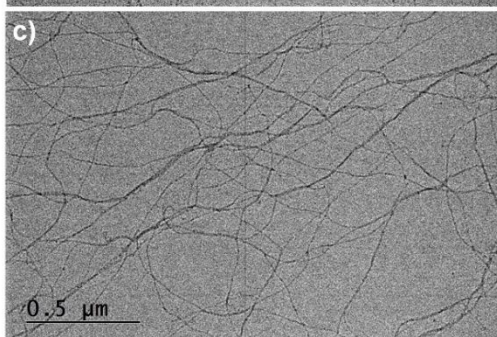
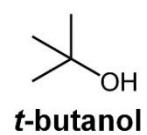
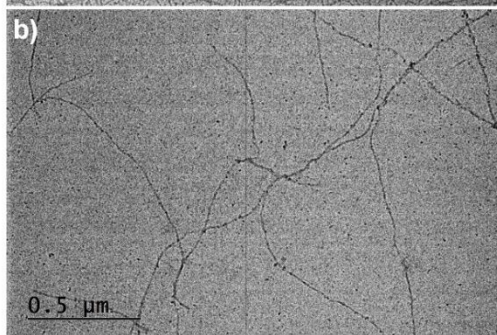
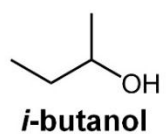
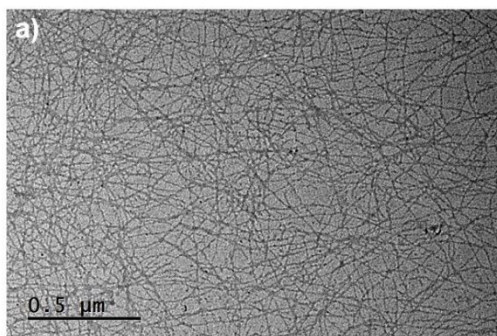
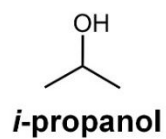


**Figure S18.** TEM images showing the formation of self-assembled nanofibrils of F6C11 (0.25 mM) in the presence of cosolvents (5 v/v%): (a) *i*-propanol; (b) *i*-butanol; (c) *t*-butanol.

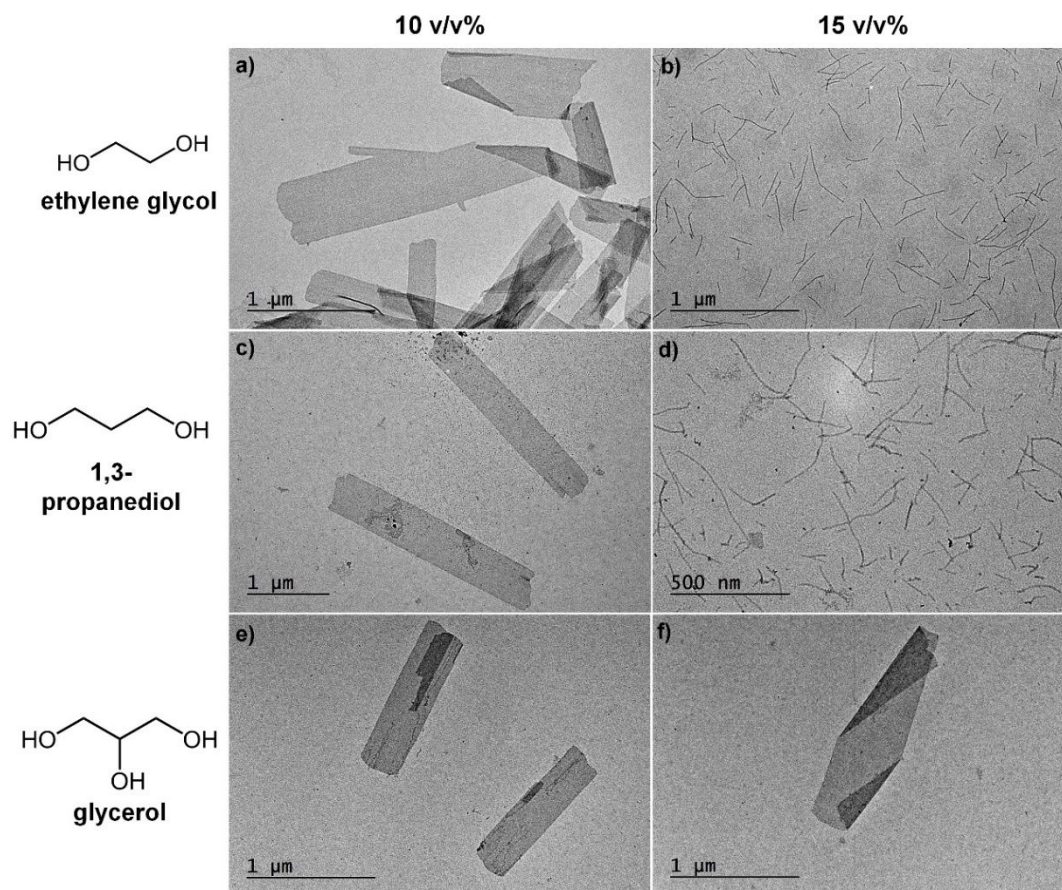


**Figure S19.** TEM images of nanosheets and nanofibrils in F6C11 solution (0.25 mM) with the addition of (a, b) ethylene glycol, (c, d) 1,3-propanediol, (e, f) glycerol. The volume concentration of cosolvents was (a, c, e) 10 v/v% and (b, d, f) 15 v/v%.

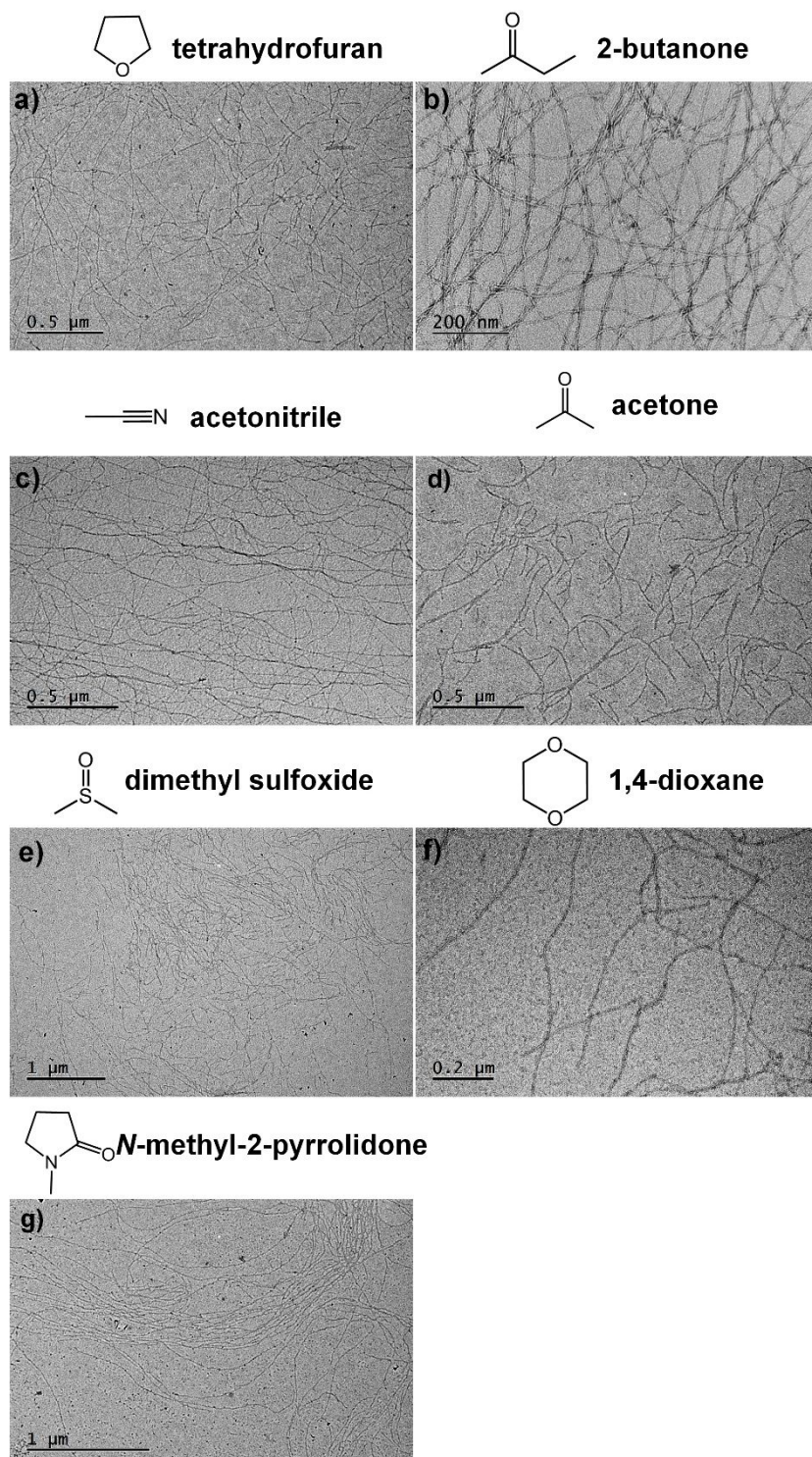


**Figure S20.** TEM images showing cosolvent-induced formation of F6C11 nanofibrils: (a) tetrahydrofuran, (b) 2-butanone, (c) acetonitrile, (d) acetone, (e) dimethyl sulfoxide, (f) 1,4-dioxane, and (g) *N*-methyl-2-pyrrolidone. The solvent content was 5 v/v% and the peptide concentration was 0.25 mM.